Brain Structure and Function (2019) 224:1871–1884
https://doi.org/10.1007/s00429-019-01881-1

ORIGINAL ARTICLE

Effects of neonatal ethanol on cerebral cortex development through adolescence

John F. Smiley[1,2] · Cynthia Bleiwas[1] · Kurt Masiello[1] · Eva Petkova[1,3,4] · Judith Betz[1] · Maria Hui[1] · Donald A. Wilson[1,3] · Mariko Saito[1,2]

Received: 20 June 2018 / Accepted: 19 April 2019 / Published online: 2 May 2019

Abstract

Neonatal brain lesions cause deficits in structure and function of the cerebral cortex that sometimes are not fully expressed until adolescence. To better understand the onset and persistence of changes caused by postnatal day 7 (P7) ethanol treatment, we examined neocortical cell numbers, volume, surface area and thickness from neonatal to post-adolescent ages. In control mice, total neuron number decreased from P8 to reach approximately stable levels at about P30, as expected from normal programmed cell death. Cortical thickness reached adult levels by P14, but cortical volume and surface area continued to increase from juvenile (P20–30) to post-adolescent (P54–93) ages. P7 ethanol caused a reduction of total neurons by P14, but this deficit was transient, with later ages having only small and non-significant reductions. Previous studies also reported transient neuron loss after neonatal lesions that might be partially explained by an acute acceleration of normally occurring programmed cell death. GABAergic neurons expressing parvalbumin, calretinin, or somatostatin were reduced by P14, but unlike total neurons the reductions persisted or increased in later ages. Cortical volume, surface area and thickness were also reduced by P7 ethanol. Cortical volume showed evidence of a transient reduction at P14, and then was reduced again in post-adolescent ages. The results show a developmental sequence of neonatal ethanol effects. By juvenile ages the cortex overcomes the P14 deficit of total neurons, whereas P14 GABA cell deficits persist. Cortical volume reductions were present at P14, and again in post-adolescent ages.

Keywords Adolescence · Neonatal · Stereology · GABA · Fetal alcohol · Programmed cell death

Introduction

In humans, cerebral cortex reaches peak volume at approximately 11 years old, after which volume and thickness decrease through adolescence (Giedd and Rapoport 2010). These changes correspond to ongoing cognitive development (Shaw et al. 2006), and their trajectory is altered in brain disorders including childhood onset schizophrenia, autism, and fetal alcohol spectrum disorders (Gogtay 2008; Lebel et al. 2012; Baribeau and Anagnostou 2013). At present, the cellular changes that accompany adolescent development of cortical shape are incompletely understood. Neurons undergo increased myelination, maturation of neurotransmitter systems, and loss of dendritic spines during adolescence (Huttenlocher and Dabholkar 1997; Petanjek et al. 2011; Catts et al. 2013). However, it is unclear to what extent these changes contribute to the reduction of cortical volume and thickness, which in normal adolescence are estimated to be as large as 10% of total cortex. To our knowledge, estimates of cortical cell number changes during human adolescence are unavailable, aside from two studies with limited samples sizes (Huttenlocher 1990; Barger et al. 2015).

Psychiatric disorders often have their onset around adolescence and are more common after pre- or perinatal complications (Brown 2011; Benros et al. 2013). Thus, it is hypothesized that early brain disruptions increase adolescent vulnerability to psychiatric disease. This is supported

✉ John F. Smiley
smiley@nki.rfmh.org

1 Nathan Kline Institute for Psychiatric Research, 140 Old Orangeburg Rd, Orangeburg, NY 10962, USA

2 Department of Psychiatry, New York University Medical Center, New York, NY, USA

3 Department of Child and Adolescent Psychiatry, New York University Medical Center, New York, NY, USA

4 Department of Population Health, New York University Medical Center, New York, NY, USA

by animal models in which early lesions cause abnormalities found in psychiatric subjects, including for example, reductions of GABA expression, dendritic length, and dendritic spine density [e.g. (O'Donnell, 2011; Komitova et al. 2013; Sadrian et al. 2014)]. These abnormalities might occur at or near the time of early lesion and precede the onset of psychiatric symptoms. Alternatively, or additionally, they could be a consequence of the disease state. For example, reduced GABA expression, dendritic length, and dendritic spine density can also be induced by stress in adult animals (Duman and Duman 2015; Ghosal et al. 2017). To distinguish these possibilities, it is of interest to know when changes associated with early lesions are first expressed.

Substantial progress has been made to establish rodent homologues of human development. The first 10 postnatal days in rodents are often used to model late gestation in humans (Ikonomidou et al. 2000; Semple et al. 2013). This is a period when most cortical neurons have finished migration, although there is some persisting neuronal migration and neurogenesis (Miller 1988; Inta et al. 2008; Miyoshi and Fishell 2011). Synapse formation is robust, and programmed cell death is maximal (Spreafico et al. 1995; Rabinowicz et al. 1996; Le Magueresse and Monyer 2013). Rodent brains grow rapidly during the first few postnatal weeks, like the human brain growth spurt in the first two postnatal years (Dobbing and Sands 1979; Hahn et al. 1983; Uylings 2000). The period around P20–P30, during which rodents are weaned but sexually immature, is sometimes referred to as the juvenile phase (Spear 2000). Adolescence occurs at approximately P30–42, defined by social, neurochemical and anatomical development (Spear 2000; Semple et al. 2013). Like humans, rodent adolescents are undergoing increased myelination, decrease of dendritic spines and maturation of neurotransmitter systems (Kim and Juraska 1997; Zuo et al. 2005; O'Donnell 2011; Suri et al. 2015; Willing and Juraska 2015). While postnatal brain development is similar in mice and rats, most of the above descriptions are from rats, and the boundaries of juvenile and adolescent phases can vary depending on the animal strain, sex, environmental conditions, and the developmental feature of interest (Spear 2000). For the present study, a working definition was adopted that included rapid growth (P8–14), juvenile (P20–30) and post-adolescent phases (P54–93). While these definitions may prove to be imprecise in future studies, the inclusion of multiple time points in each phase gave us confidence that our data captured the broad trends of postnatal neocortex development into early adulthood.

We investigated neocortical development after subcutaneous ethanol injections at P7, using the treatment paradigm developed by Olney and colleagues (Ikonomidou et al. 2000). Since their seminal work, this method has been widely used as a model of fetal alcohol spectrum disorder corresponding approximately to ethanol exposure in the third trimester of human fetal development [e.g. (Wozniak et al. 2004; Kumral et al. 2005; Ieraci and Herrera 2007; Noel et al. 2011; Wilson et al. 2011; Coleman et al. 2012; Subbanna et al. 2013; Susick et al. 2014; Wagner et al. 2014; Smiley et al. 2015; Hamilton et al. 2016; Wilson et al. 2016; Lewin et al. 2018; Saito et al. 2018)]. A significant advantage of this model is that it provides precise control of the timing of ethanol exposure, to help isolate the effects of binge-like ethanol exposure at a defined developmental stage. It has similarities with other models that disrupt this sensitive developmental timepoint, for example, using NMDA antagonists, hypoxia, hyperoxia, heavy metals, or surgical lesions of the ventral hippocampus (Ikonomidou et al. 2000; Dribben et al. 2011; O'Donnell 2011; Komitova et al. 2013; Nikolic et al. 2013; Reich et al. 2016). In adults, P7 ethanol causes behavioral deficits (Wozniak et al. 2004; Coleman et al. 2009; Wilson et al. 2011, 2016; Hamilton et al. 2016; Lewin et al. 2018) and anatomical changes including reduced GABA cells, dendritic length, dendritic spines, and cortical volume (Granato, 2006; Coleman et al. 2009, 2012; Hamilton et al. 2015; Smiley et al. 2015; Saito et al. 2018). Immediately after P7 ethanol, there is widespread apoptotic cell death in the cerebral cortex, that peaks about 8 h after treatment (Olney et al. 2002b). Curiously, although apoptotic markers are obviously abundant in both pyramidal and GABA neurons (Saito et al. 2018) adult cortex has large deficits of GABA neurons but small deficits of total neuron number (Smiley et al. 2015) suggesting that pyramidal neurons have greater capacity than GABA neurons to compensate for neonatal cell loss. Additionally, there is evidence that GABA reductions may be caused not only by cell death, but also by later downregulation of the GABAergic phenotype in surviving cells (Saito et al. 2018). Thus, one goal of the present study was to determine the onset and persistence of pyramidal and GABA cell deficits after ethanol treatment.

Methods

Subjects and ethanol exposure

Data are presented from 124 C57BL/6By mice. Ethanol and saline injected animals were compared at eight different developmental time-points from P8 to P93. The number of animals used for the different measurements at each time point is shown in Table 1. At each time-point, the ethanol-treated animals were matched with saline-treated animals by litter and by sex. To reduce litter effects, multiple litters were included within each treatment group.

All mice were subcutaneously injected at P7 with either saline or ethanol, with two injections separated by a 2-h interval. Each ethanol injection applied a dose of 2.5 g/kg

Table 1 Number of animals used (Females)

Age	Phase	All other measurements		Parvalbumin		Calretinin		Somatostain	
		SAL	ETOH	SAL	ETOH	SAL	ETOH	SAL	ETOH
P8	Rapid growth, early	8 (4)	8 (4)						
P11	Rapid growth, early	4 (2)	4 (2)						
P14	Rapid growth, late	12 (5)	12 (5)	12 (5)	12 (5)	12 (5)	12 (5)	4 (3)	4 (3)
P20	Juvenile	11 (6)	10 (6)	11 (6)	10 (6)	11 (6)	10 (6)	4 (2)	3 (0)
P30	Juvenile	6 (3)	6 (3)	6 (3)	6 (3)	6 (3)	6 (3)	2 (1)	2 (1)
PS4	Post-adolescent	8 (6)	8 (4)	8 (6)	8 (4)	8 (6)	8 (4)		
P70	Post adolescent	5 (3)	5 (2)	5 (3)	5 (2)	5 (3)	5 (2)	5 (3)	5 (2)
P93	Post adolescent	8 (4)	9 (4)	8 (4)	9 (4)	8 (4)	9 (4)		
Total		62 (33)	62 (30)	50 (27)	50 (24)	50 (27)	50 (24)	15 (9)	14 (6)

that was previously shown to induce peak blood ethanol of ~ 0.5 g/dL after the second injections, as measured in truncal blood (Ikonomidou et al. 2000; Saito et al. 2007). After injections pups were returned to their litter, and weaning occurred at P25–30. This dose of ethanol is well tolerated by pups, with 96% survival rate at P90 in a sample of ethanol-injected animals ($n = 105$) similar to 97% survival in saline-treated animals ($n = 131$). Previous measurements showed that this treatment had only slight and non-significant effects on body weight at juvenile or adult ages (Coleman et al. 2012; Sadrian et al. 2014). All procedures were approved by the Nathan Kline Institute IACUC and were in accordance with NIH guidelines for the proper treatment of animals.

Histological processing and immunolabeling

Mice were anesthetized by intraperitoneal injection of 200 mg/kg ketamine plus 10 mg/kg xylazine, and transcardially perfused with heparinized 4% paraformaldehyde in phosphate buffer, pH 7.2. Brains were removed from the skull and immersed in the same fixative at 4C for 24 h before short-term storage in phosphate buffer with 0.02% sodium azide.

As in our previous study (Smiley et al. 2015) brains were embedded in blocks for simultaneous sectioning and processing, so that matched ethanol and saline-treated brains at each developmental age were always processed in the same tissue sections, with each block containing from 6 to 16 brains (Fig. 1). While we previously embedded brains in a protein matrix for simultaneous processing (Smiley and Bleiwas 2012), in the present study we used a less complicated agar embedding method (Nagamoto-Combs et al. 2016) with slight modifications. Briefly, fixed brains were sunk in 20% buffered glycerol, and then immersed for 1 h at 40C in 15% agar in phosphate buffered saline as in the published protocol, but additionally adding 15 grams of sucrose to each 100 ml agar solution so that the final frozen block was softer and easier to cut, and also adding 2% (vol/vol) commercially available red food coloring to increase agar-tissue contrast for block-faced imaging (Smiley and Bleiwas 2012). Brains were then pinned through the brainstem onto a base of hardened agar, carefully aligned for coronal sectioning, and immersed in the same agar-sucrose solution described above and left to cool several hours at 4C. Once hardened, the block was trimmed to size, immersed overnight in 4% formalin at 4C, and then cryoprotected by sinking in 20% buffered glycerol, prior to freezing and then sectioning in coronal orientation at 50um thickness on a sliding microtome.

Free-floating sections were used for all immunolabeling procedures. Primary antibodies included mouse anti-neuron specific protein (NeuN; Millipore catalog # MAB377) used at 1:2,000, mouse anti-parvalbumin (PV; Sigma catalog # P3088) used at 1:2,500, rabbit anti-calretinin (CR; Swant catalog # 7699/4) used at 1:5,000, rabbit anti-somatostatin-14 (Peninsula catalog # T-4103) used at 1:2,000, rabbit anti-cleaved caspase-3 (CC3; Cell Signaling catalog # 9664) used at 1:400, and rat anti-Ctip2 (Abcam catalog # 18465) used at 1:300. For immunofluorescence, primary antibodies were visualized with Alexa Fluor 488- or 594-conjugated secondary antibodies (Invitrogen catalog # A11001 or #A11008), cell nuclei were stained by immersing sections for 20 min in 200 nM 4′6′diamino-2-phenylindole (DAPI; Sigma catalog # D9564) and sections were mounted on glass slides coverslipped using Fluoro-Gel aqueous mounting medium (Electron Microscopy Sciences, catalog # 17985-s10). CR neurons were labeled using the streptavidin–biotin–peroxidase method with diaminobenzidine reaction product, after which sections were dried on chrome-alum slides before dehydration and cover-slipping with Permount. Nissl stained sections were dried on slides before staining with thionin and cover-slipping with Permount.

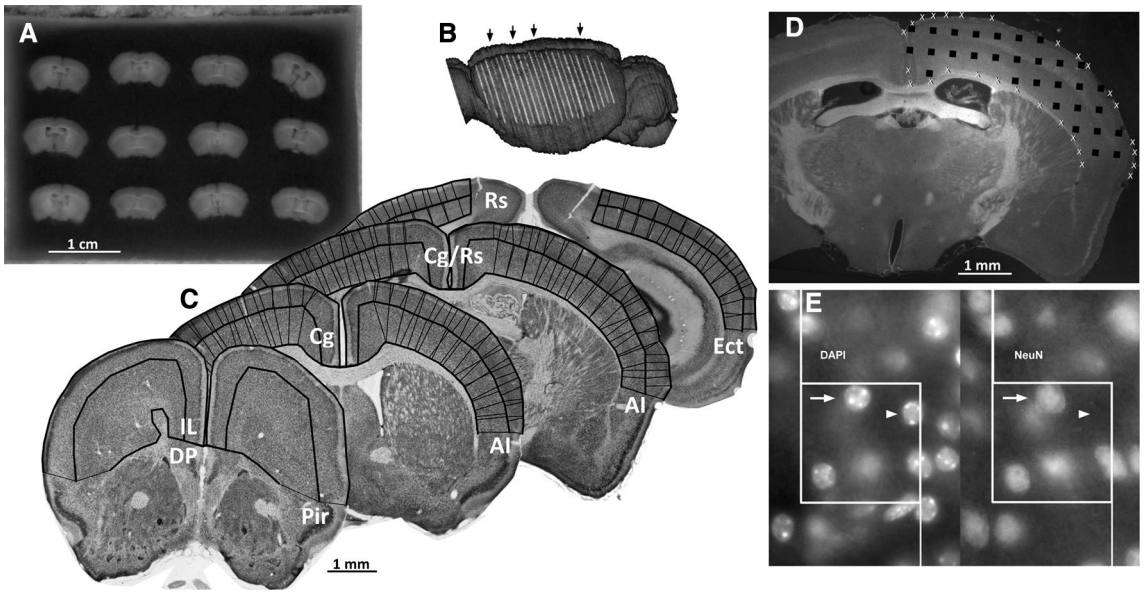

Fig. 1 The methods used for quantitative morphometry are illustrated. **a** Matched ethanol and control brains at each time-point were simultaneously processed by embedding in an agar block. Shown is a block face image taken during sectioning, that was acquired for each section. **b** A 3-dimensional reconstruction is shown that was made from the block faced images taken at sectioning. White lines show the region of the neocortex that was sampled on each 6th section for measurements of cortical thickness, surface area and volume. Typically, 18–22 sections were sampled from each brain for these measurements. Black arrows indicate the location of the sections shown in **c**. **c** Sample Nissl stained sections demonstrate the regions of neocortex that were included in different measurements. The thick black outlines show the tracings of the pial surface, white matter borers, and layer IV/V border that were used for volume and surface area measurements, as well as for cell counting. These measurements included the midline infralimbic and cingulate areas but excluded the retrosplenial cortex in caudal sections where the hippocampus was present. Thin vertical lines are shown at areas measured for cortical thickness. To avoid tangentially cut rostral cortex, thickness measurements were not taken from the sections more than one section rostral from the anterior commissure. To avoid midline distortions, thickness measures were not taken from midline cingulate areas. **d** For stereological cell counts, a systematically random placed grid of counting sites (black squares) was sampled in the left neocortex. **e** To estimate total cortical neuron numbers, identically focused z-stacks were obtained at each disector site, and these were simultaneously displayed for counting. DAPI cell that contained NeuN (arrow) were counted as neurons, and those that lacked it (arrowhead) were counted as non-neuronal cells. Counting box width = 34 microns. *AI* agranular insular cortex, *Cg* cingulate cortex, *DP* dorsopeduncular cortex, *Ect* ectorhinal cortex, *IL* infralimbic cortex, *Pir* piriform cortex, *Rs* retrosplenial cortex

Quantitative morphometry

Anatomical measurements were done using methods previously described, with some modifications (Smiley et al. 2015). Briefly, whole fixed brain volumes were measured by a fluid displacement method before histological embedding (Dorph-Petersen et al. 2005). All histological measurements were done in neocortex, thus omitting areas of archicortex and paleocortex (Fig. 1). For measurement of neocortex volume, surface area and thickness, ImageJ software was used to trace the countours of pia and white matter boundaries on every 6th coronal Nissl stained section, viewed on digital images obtained with a ×2 microscope objective at final magnification of 310 pixels per millimeter. To search for hemispheric asymmetries, these cortical shapes were measured separately in the left and right hemispheres. Thickness measurements were displayed as colored flat maps to visualize regional distributions (Smiley et al. 2009, 2015).

Neuron numbers were estimated in the left neocortex using the optical disector method (Gundersen et al. 1988). Neocortex was sampled on every 12th section through neocortex with systematic random grids of sampling sites, and at each site a z-stack of six 2-um spaced images was captured with a Foculus FO442 digital camera (Net GMBH, Germany), using a 40×, 1.3 numerical aperture (NA) oil-immersion objective for fluorescent sections, and a 50×,1.3 NA oil-immersion objective for peroxidase labeled CR cells. Cell counting was done on optical disector counting boxes drawn onto each z-stack, with the upper guard zone of two z-stack images, a counting box of three images, and a bottom guard zone of one image. However, for CR immunolabeled sections, that had on-slide thickness of 9–14 microns, we used only one image (2 microns) for the upper guard zone.

In CR counts, we were careful to omit pyramidal cells in middle cortical layers that were CR-immunolabeled in P8–14 animals (Melvin and Dyck 2003). Additionally, we omitted the CR cells in deep layers near the midline corpus

callosum that were easily distinguished by their dense label, small round soma, and irregularly shaped proximal dendrites that contrasted with the straight dendrites of most CR neurons (Revishchin et al. 2010).

To estimate total numbers of neurons and non-neuronal cells, identically focused z-stacks of NeuN labeling and DAPI-labeled nuclei were obtained at each disector site. Both labels were simultaneously displayed, and DAPI nuclei that also expressed NeuN were counted as neurons. The same disectors were used to estimate the number of non-neuronal cells identified as DAPI nuclei that lacked NeuN. The latter included glia, as well as blood vessel associated endothelial and smooth muscle cells. While NeuN labeling was robust even at younger ages, it was previously shown that some neurons do no express this marker, although the most obvious examples were in brain areas other than cerebral cortex [e.g., (Cannon and Greenamyre 2009; Duan et al. 2016)].

To estimate cell numbers, typical X–Y counting box dimensions were 200 µm × 144 µm for GABA cells, and 34 µm × 34 µm for NeuN and DAPI cells. Disector spacing was adjusted so that the average number of disectors per cell number estimate was 239 ± 55 (mean ± SD) and the average coefficient of error (Dorph-Petersen et al. 2009) was 0.082 ± 0.031 ($N = 537$ estimates of cell number). Coefficients of error rarely exceeded the acceptable threshold of 0.1, although they were 0.15 ± 0.03 for PV cells at P14 where comparatively few cells were detectable.

Cortical volumes were estimated using the Cavalieri method (Gundersen et al. 1999). For calculation of cell numbers, we multiplied cell densities by cortical volumes obtained from the same sections used for cell density measurements. This approach differed from our previous study, that used volumes from Nissl sections for all cell number calculations (Smiley et al. 2015). In the present study, we realized that volume measurements from immunofluorescence and immunoperoxidase processed section were as much as 15% reduced compared to those of Nissl sections. Therefore, the reported cell numbers in the present study are lower than previously reported.

All calculations of cell number were corrected for section thickness that was measured in triplicate on every section used for cell counting. For immunoperoxidase-labeled CR sections, the on-slide thickness was 11.0 ± 1.4 µM ($N = 112$ brains) and did not differ between treatment groups ($p = 0.97$, T test). For immunofluorescence sections, coverslipped with Fluor-Gel aqueous mounting media (Electron Microscopy Sciences, cat. # 17985-s10), slides were stored in a humidified chamber at 4C and imaged for cell counting within 10 days of mounting, to minimize possible on-slide shrinkage. Sections thickness was measured to be 50.0 ± 3.5 uM thick, with no significant difference between treatment groups ($p = 0.93$). The thickness measurements were not corrected for refractive index mismatch caused using an oil immersion objective with an aqueous sample, and thus overestimate section thickness by 15–20% (Hell et al. 1993; Dorph-Petersen et al. 2001). The effect of this distortion on the estimate of final cell density is theoretically minimized by the simultaneous overestimate of the counting box depth.

Statistics

The present study was designed to determine the developmental onset and persistence of effects of neonatal ethanol treatment. For statistical comparisons of all measurements except GABA cell numbers, samples were divided into 4 developmental phases (Table 1). Previous authors considered P8–14 to be in the phase of rapid brain growth (Dobbing and Sands 1979; Hahn et al. 1983). For the present study we subdivided this phase of rapid growth into early ages when P7 ethanol effects were just beginning (P8–11), and 1-week post-treatment when most measurements showed a clear effect of ethanol (P14). Animals at P20–30 were included in a juvenile phase, and animals at P54–93 were included in a post-adolescent phase (Spear 2000; Schneider 2013). For analyses of GABA cell numbers, only the later 3 developmental phases were included because these cells were poorly detected at P8–11. Analyses were done using a three-way univariate analysis of variance (ANOVA) using the general linear model implemented in the IBM SPSS version 24 program, with treatment (2 levels), developmental phase (4 or 3 levels) and sex (2 levels) included as predictor variables. Sex was included because there is precedence for sex differences in brain development; note that our samples contained nearly equal numbers of males and females. Comparisons between treatment groups at the individual developmental phases, or between the developmental phases in control animals, used significance thresholds that were Bonferroni-corrected for the number of developmental phases (usually 4, or 3 for GABA cell numbers). We additionally considered an alternate statistical model that included only 3 developmental phases for all measurements, omitting the P8–11 measurements because they could be considered "baseline" when ethanol effects were still very minor. However, estimates and significance of the main effects and interactions were nearly identical in both models, and since the results did not differ this latter model is not presented.

All measurements were done on coded images so that raters were blind to treatment group. Results that are expressed as percent changes for comparisons between treatment groups were calculated as = 100 × (1 − ethanol/saline), between ages as = 100 × (1 − older/younger), and between sexes as = 100 × (1 − female/male).

Results

Figure 2 illustrates the abundant apoptosis in cortical neurons that occurs within hours of P7 ethanol injection. Both pyramidal and non-pyramidal shaped neurons expressing CC3 immunoreactivity are widely distributed across the regions and layers of neocortex. Double labeling with Ctip2, a marker for deep layer cortical projection neurons, confirms that many CC3 neurons are pyramidal cells. Previous studies using the same ethanol treatment in P7 mice concluded that this pattern of CC3 expression indicates widespread cell death by apoptosis, without obvious evidence of non-apoptotic excitotoxic cell death (Olney et al. 2002a).

Total cell numbers

Total cell numbers were estimated in all brains available from P8 to P93 (Table 1). Neuron number was estimated by counting DAPI-labeled cells that colocalized NeuN immunolabeling, and non-neuron number by counting DAPI-labeled cells that lacked NeuN. In control animals, total neuron number decreased from the phase of early rapid growth (P8–11) to the juvenile phase (P20–30; $p = 0.016$, which is trend-level for Bonferroni-corrected significance; Fig. 3) consistent with ongoing programmed cell death in this period (see Discussion). In the same time-period, the number of non-neuronal cells increased ($p < 0.001$; Fig. 3) consistent with ongoing gliogenesis and angiogenesis (Semple et al. 2013). Overall, comparing the earliest time-point measured (P8) to the time when total cell numbers become approximately stable (P30), total neuron number decreased by 14%, whereas non-neuronal cell number increased 48%. Subsequently, comparing juvenile to post-adolescent ages, there were no further significant changes in neuronal or non-neuronal numbers, indicating that ongoing cortical volume increase at the same time is not caused by increasing cell number.

P7 ethanol caused a reduction of total neuron number. Three-way ANOVA showed significant main effects of both ethanol treatment ($F(1,108) = 12.1$, $p < 0.001$) and developmental phase ($F(3,108) = 4.9$, $p = 0.003$) and a significant interaction between treatment and phase ($F(3,108) = 2.9$, $p = 0.04$). Analysis of individual developmental phases showed that the ethanol effect was significant at P14 ($F(1,20) = 23.2$, $p < 0.001$). However, the 18% reduction due to ethanol at this developmental phase appeared to be transient, followed by smaller and non-significant ethanol-related reductions at juvenile (2%) and post-adolescent phases (7%; Fig. 4a). The lower neuron number in ethanol-treated P14 animals was not explained by a simple down-regulation of NeuN-immunoreactivity, as there was not a concurrent increase of non-neuronal cell counts (Fig. 4b).

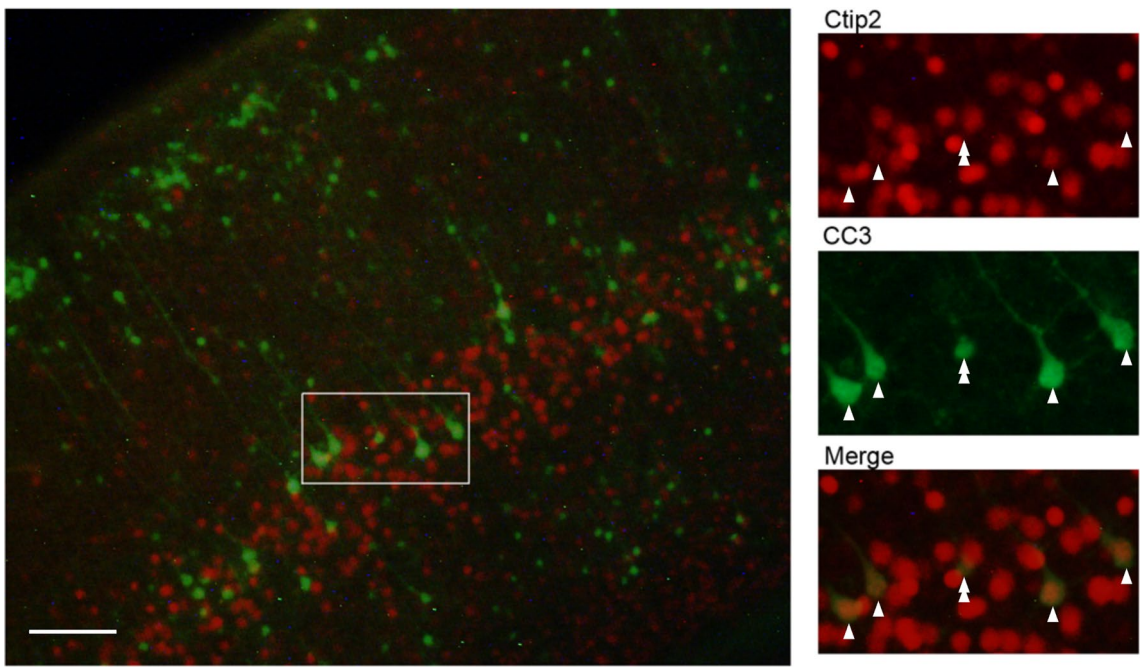

Fig. 2 Immunolabeling for cleaved caspase-3 (CC3) 8 h after P7 ethanol injections shows the distribution of apoptotic cells in mouse somatosensory cortex. CC3 neurons (green label) are present in all layers, although more abundant in layers II and V. Cells with both pyramidal and non-pyramidal morphology are present. Inset: pyramidal cell identity was confirmed in many cells by colocalized Ctip2 label (arrowheads, red label). Some cells did not colocalize (double arrowhead). Scale bar = 100um

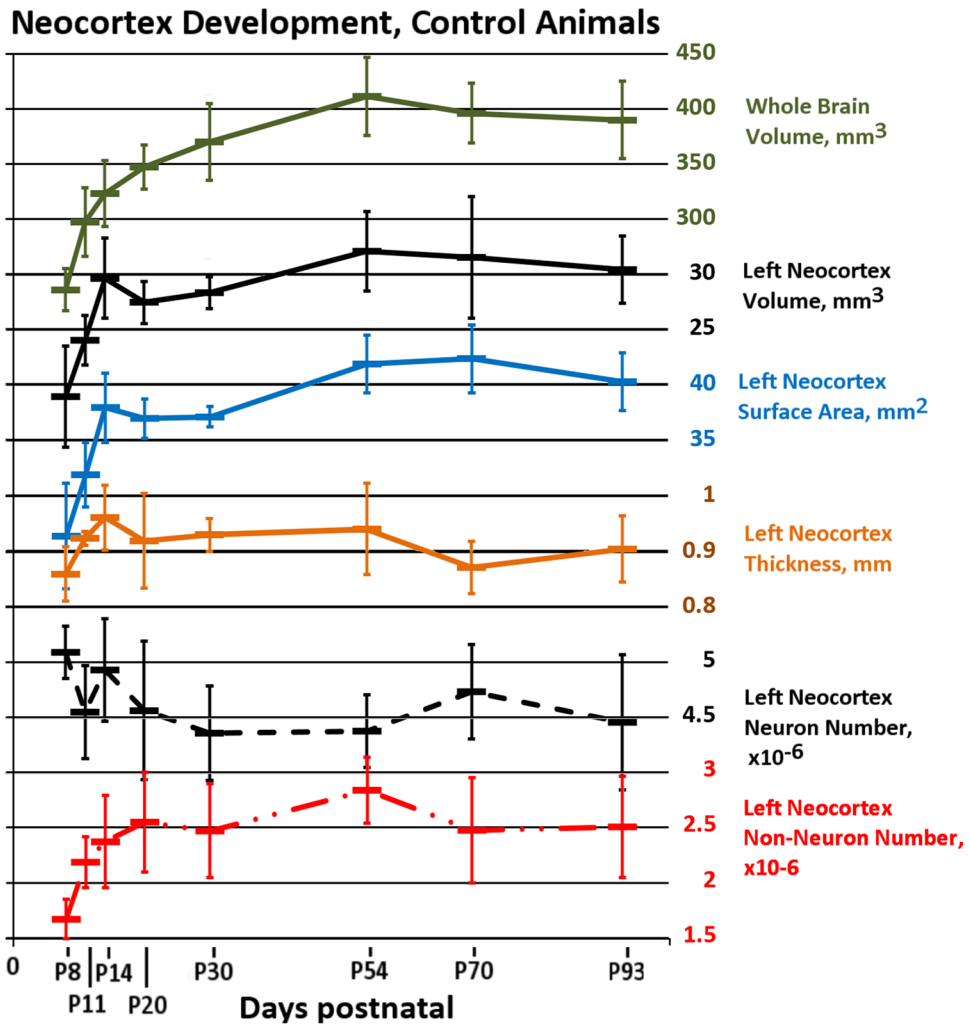

Fig. 3 As shown in data from control animals, different features of whole brain and neocortex have distinct developmental trajectories. Whole brain volume, neocortex volume and surface area all grow rapidly until about P14, and then continue to increase more gradually until about 54. In contrast, neocortical thickness reaches a plateau as early as P14. Total neuron number decreases from P8 to reach approximately stable levels by about P30. Non-neuron number increases rapidly from P8 to about P20, after which it remains approximately stable. Non-neuron number includes all glia and endothelial cells that are DAPI-labeled but lack NeuN immunolabeling. Error bars = standard deviations

P7 ethanol also caused a reduction of non-neuron number (Fig. 4b). Three-way ANOVA showed significant effects of both treatment ($F(1,108) = 5.3$, $p = 0.02$) and developmental phase ($F(3,108) = 17.7$, $p < 0.001$). The main effect of treatment was due to reduced cell numbers ranging from 3% (at P20–30) to 11–13% (at P14 and P54–92). Interactions of treatment with developmental phase or with sex were not significant. However, there was a significant interaction between sex and developmental phase ($F(3,108) = 3.8$, $p = 0.013$). Further analsyis showed that this was due to 15% more non-neuronal cells in males than females at the post-adolesecent phase, whereas a similar difference was not present at earlier phases. This sex difference was similar in ethanol and saline-treated animals.

GABA neuron numbers

PV and CR neuron counts are presented from all animals P14 and older, whereas somatostatin neurons were sampled in fewer animals (Table 1). At P8–11 comparatively few PV and CR cells were clearly detected by immunolabeling. Strong cell labeling, and cell counts approaching mature (e.g., post-adolescent) levels were first obtained at P14 for CR, and not until P20 for PV. Somatostatin cells were already near post-adolescent levels by P14, which was the earliest time they were sampled.

P7 ethanol caused a clear reduction of all three GABA subpopulations (Fig. 5). For PV cells, three-way ANOVA showed significant main effects of treatment ($F(1,88) = 34.2$, $p < 0.001$) and developmental phase ($F(1,88) = 155.5$, $p < 0.001$), but there was no significant interaction between treatment and phase ($F(2,88) = 0.44$, $p = 0.65$). The effect of phase was due to the low cell counts obtained at P14 compared to later phases. Even though cell counts were low at P14, there was already evidence of an ethanol-related reduction (32%), similar to the reductions at subsequent phases (19%).

Analysis of CR cells showed a significant effect of treatment ($F(1,88) = 32.9$, $p < 0.001$) and developmental phase ($F(1,88) = 8.2$, $p < 0.001$) and there was a trend-level

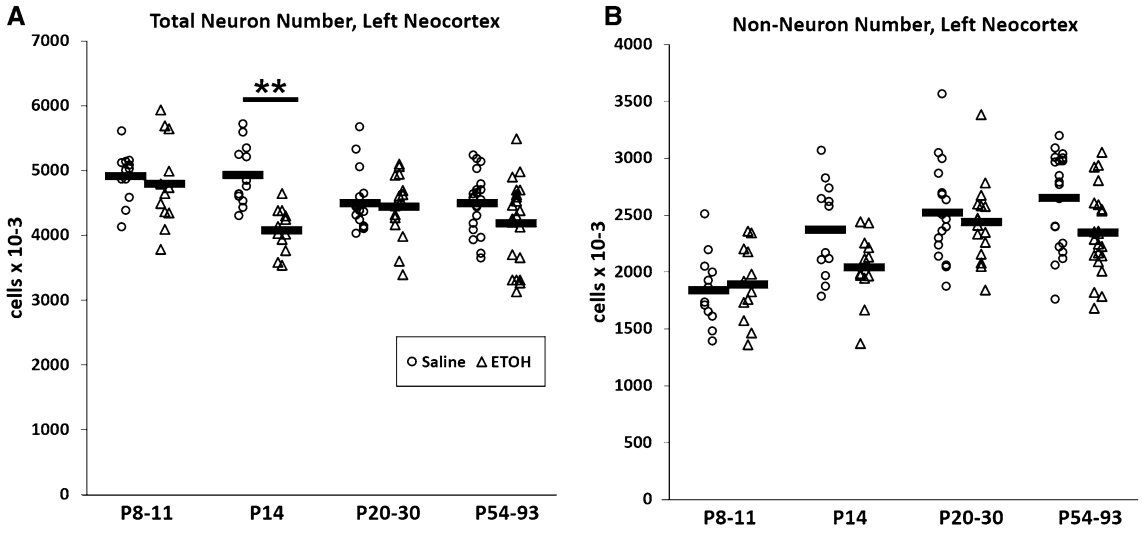

Fig. 4 Total cell numbers were estimated in left neocortex in control animals (open circles) and ethanol treated animals (open triangles), at four developmental phases. **a** Total neuron number was significantly reduced only at P14. This decrease was transient, with only small and non-significant reductions in subsequent phases. **b** While the three-way ANOVA showed an overall significant reduction of non-neuronal cells, comparisons at individual developmental phases did not show any significant differences. Asterisks indicate statistical differences between treatment groups at individual developmental phases, that were Bonferroni corrected for multiple comparisons (**$p < 0.0025$)

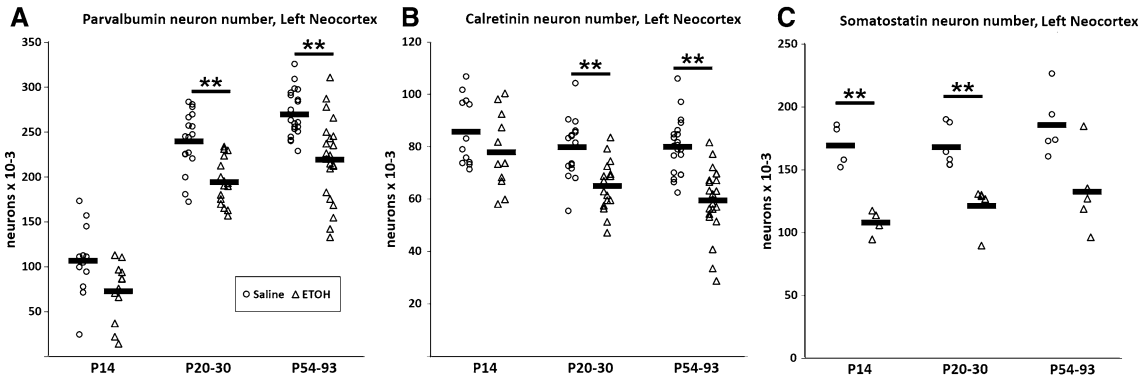

Fig. 5 GABA cell numbers were estimated in the left neocortex in control animals (open circles) and ethanol treated animals (open triangles), at three different developmental phases. GABA cells were not evaluated before P14 due to poor immunolabeling in some cells. **a** ANOVA analysis of PV cell counts showed a significant main effect of treatment, but no evidence for an interaction between ethanol treatment and developmental phase. However, at P14, the number of detectable cells was low due to immature expression of PV immunolabeling, and although the PV cell counts were 32% lower in ethanol-treated brains, the 2-sample *t* test did not reach Bonferroni corrected significance ($p = 0.033$). The ethanol effect on PV cell number estimated with 2-sample *t* test was similar and significant at juvenile (19%) and post-adolescent (19%) phases. **b** ANOVA analysis of CR cell counts showed a trend-level significance for the interaction between treatment and developmental phase: ethanol treated animals had smaller reductions at P14 (9%) compared to juvenile (19%) and post-adolescent (26%) phases. **c** ANOVA analysis of Somatostatin neuron counts showed a significant main effect of treatment. Ethanol treatment caused similar reductions (29–36%) at all three developmental phases. Asterisks indicate statistical differences between treatment groups at individual developmental phases, based on 2-samples *t* test, that were Bonferroni corrected for multiple comparisons (**$p < 0.0025$)

interaction between treatment and phase ($F(2,88 = 2.5$, $p = 0.08$). The interaction was caused by progressively larger ethanol-related reduction from P14 (9%) to P20-30 (19%) to P54-93 (26%). The main effect of developmental phase was caused by progressively decreasing cell numbers in older animals, mainly in the ethanol-treated animals.

Three-way ANOVA for somatostatin cells showed a main effect of ethanol treatment ($F(1,17) = 41.6$, $p < 0.001$), but no significant main effect for developmental phase, and no interaction effects. The ethanol-induced reductions in the three phases were in the range of 28–36%.

Neocortex volume, surface area, and thickness

While neocortical volume, surface area, and thickness were separately evaluated in the left and right hemispheres, there was no significant hemispheric asymmetry at any age, in either saline or ethanol injected animals. For simplicity, the following presentation of neocortical measures includes only results from the left hemisphere.

In saline-injected control animals, the developmental trajectories of neocortical volume and surface area were similar to that of whole brain volume (Fig. 3). They increased rapidly from P8 to P14, and then more gradually until about P54. Neocortical thickness also increased rapidly until P14, but then did not subsequently increase. Comparing juvenile (P20–30) to post-adolescent (P54–93) phases, neocortex volume, surface area, and whole brain volume all significantly increased by 12–13% ($F(1,36) > 13.1$, p values < 0.001), whereas thickness showed evidence of a slight but non-significant decrease.

P7 ethanol caused a reduction of neocortex volume (Fig. 6b). A three-way ANOVA that included developmental phase, treatment and sex showed a significant effect of treatment ($F(1,108) = 17.6$, $p < 0.001$) and developmental phase ($F(3,108 = 31.7$, $p < 0.001$) and a significant interaction between ethanol treatment and development ($F(3,108 = 2.9$, $p = 0.04$). Analysis of the individual phases showed that

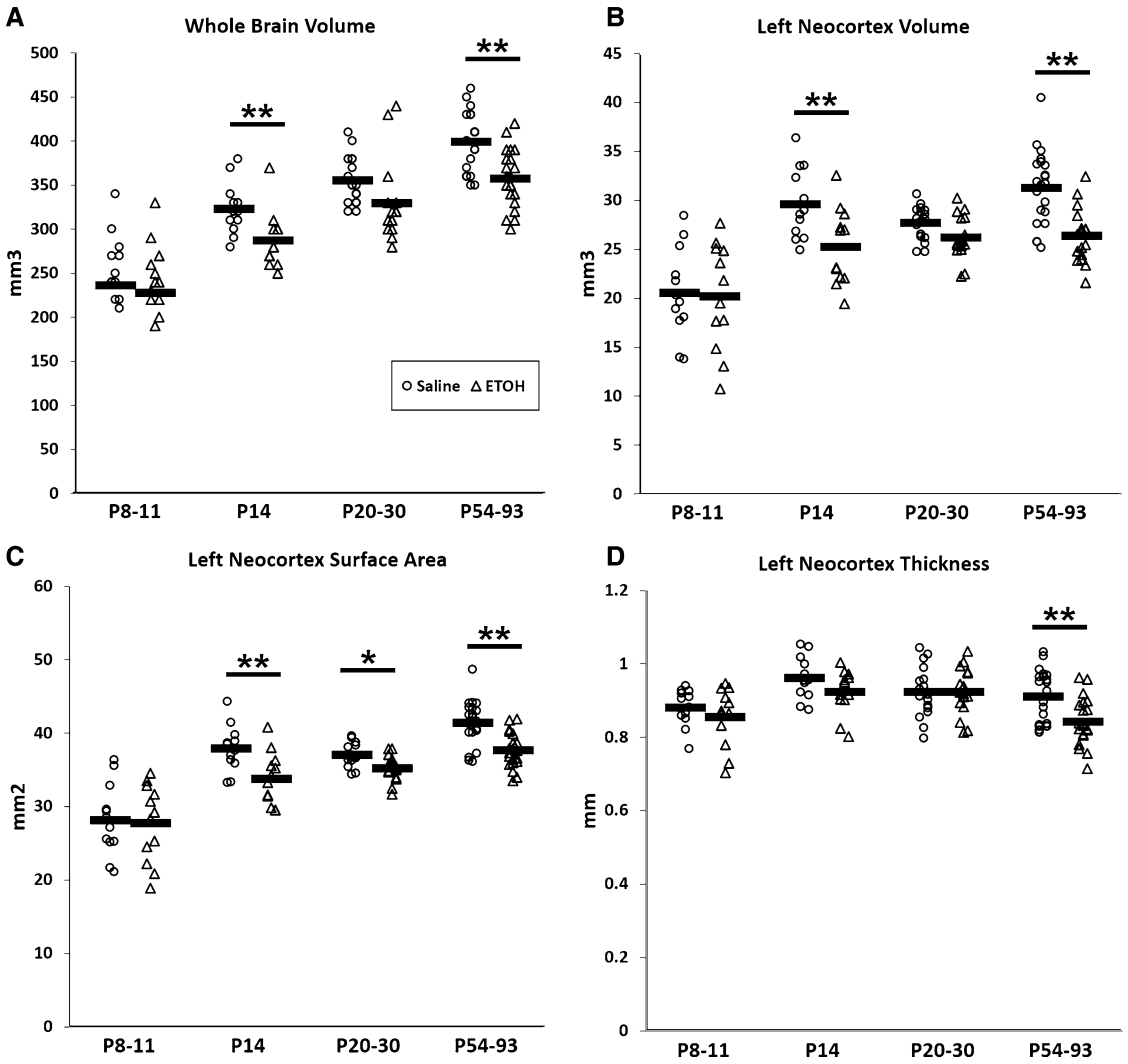

Fig. 6 Measurements of cortical volume, surface area and thickness were made at four developmental phases, in control animals (open circles) and ethanol treated animals (open triangles). **a** Whole brain volumes were reduced by P7 ethanol exposure as early as P14. **b** The effect of P7 ethanol on neocortex volume was especially pronounced at P14 and in post-adolescent animals. **c**. Neocortical surface area was reduced as early as P14. **d** The ethanol effect on neocortical thickness was most evident in post-adolescent animals. Asterisks indicate statistical differences between treatment groups at individual developmental phases, based on 2-samples t tests, that were Bonferroni corrected for multiple comparisons (*$p < 0.0125$, **$p < 0.0025$)

ethanol caused 15–16% reductions at P14 ($p = 0.009$) and at P54–93 ($p < 0.001$) whereas the 5% reduction at P20–30 did not reach Bonferroni adjusted statistical significance ($p = 0.04$). There was additionally a trend-level effect of sex ($F(1,108) = 3.6$, $p = 0.06$) due to 4% larger neocortex volumes in male animals, but there were no significant interactions between sex and treatment or developmental phase.

The effect of neonatal ethanol on whole brain volume was similar to its effect on neocortex volume (Fig. 6a). For whole brain volume, there were significant effects of ethanol treatment ($F(1,108) = 19.0$, $p < 0.001$) developmental phase ($F(3,108) = 73.3$, $p < 0.001$) and sex ($F(1,108) = 4.3$, $p < 0.04$) but none of the 2- and 3-way interactions were significant. The magnitude of the ethanol effect on brain volume was 7% at P20–30 and 11–12% at P14 and P54–93. The sex effect was due to 5% larger brain volumes in male animals.

Changes in neocortical volume can be caused by changes in its thickness and/or surface area. These parameters have different developmental profiles (Figs. 3 and 6c–d) and might reflect somewhat different aspects of cellular development in the cortex. Analysis of surface area showed a significant effect of treatment ($F(1,108) = 17.2$, $p < 0.001$) and developmental phase ($F(3,108) = 65.2$, $p < 0.001$). Similarly, analysis of cortical thickness showed an effect of treatment ($F(1,108) = 6.5$, $p = 0.012$) and developmental phase ($F(3,108) = 8.5$, $p < 0.001$). Neither measurement showed a significant sex difference or significant interactions. These measurements confirm previous results in P70 mice (Smiley et al. 2015). In that study P7 ethanol caused 14% lower neocortex volume, due to 8% reduced surface area plus 6% reduced thickness. In the present study, post-adolescent animals had 16% lower volume caused by 9% reduced surface area and 7% reduced thickness.

Discussion

We encountered three main findings by tracking the effects of neonatal ethanol during development. The first is that GABA cell reductions were already present by P14, as early as they could be measured after P7 ethanol. These reductions subsequently persisted, and only CR cell counts showed trend-level evidence for greater reductions at later stages. Second, while total neuron number was decreased at P14, this effect was transient and no longer present by the juvenile phase. Other studies also observed a transient reduction of neuron number after neonatal lesions, and we suggest that this may be partially explained by a temporary acceleration of ongoing programmed cell death. Finally, neonatal ethanol caused reductions of cortical volume, thickness and surface area. Volume measurements showed some evidence for a transient reduction at P14, like neuron number. However, unlike reduced neuron number, cortical volume deficits were also clearly present in post-adolescent animals.

Our data in the control animals show that cortical volume and surface area, like whole brain volume, continue to increase from pre-adolescence to early adult ages. We have not identified the cellular changes that contribute to this growth. Possible candidates include increasing dendritic complexity, as seen in pyramidal cells during this period in rats (Markham et al. 2013), increasing myelin volume, in conjunction with increasing white matter volume (Juraska and Willing, 2016) or increased volume of non-neuronal cells. Our cell counts did not show increasing numbers of either neuronal or non-neuronal cells that coincided with the adolescent increase of volume. Previous counts of cortical neurons also did not find increases (e.g., (Heumann et al. 1978; Lyck et al. 2007; Bandeira et al. 2009) and in fact there is evidence for a modest reduction at adolescence in prefrontal areas of female rats (Juraska and Willing, 2016). It is possible that we did not detect this modest change because we sampled whole neocortex.

The effect of neonatal ethanol on cortical volume was pronounced at P14 and in the post-adolescent phase, whereas the intevening juvenile phase showed a smaller reduction that was not significant. This developmental sequence is complex and needs to be confirmed in future studies. It suggests that neonatal ethanol has multiple effects on cortical volume. At P14, it is possible that the transient volume reduction is caused by the transient reduction of cortical cell number at this stage. Explanations for the delayed volume reduction in post-adolescent animals are more speculative. It is possible that early disruption of GABA neurotransmission causes later disruption of cortical growth. GABA neurotransmission is known to dynamically interact with different aspects of cortical maturation (Southwell et al. 2010; Le Magueresse and Monyer, 2013). It is possible that neonatal ethanol inhibits ongoing growth of cell size, as well as dendritic and axonal complexity during adolescence. Adult animals treated with neonatal ethanol have reduced dendritic length and spine density (Granato et al. 2003; Lawrence et al. 2012; Hamilton et al. 2015) and human fetal alcohol subjects have reduced white matter (Archibald et al. 2001). However, we are unaware of studies that tracked the developmental onset of these ethanol-induced effects.

Our counts of GABA neurons showed that the number of detectable cells was reduced soon after ethanol treatment, and the reduction remained stable or modestly increased by early adulthood. One explanation of these results is that many GABA cells are killed by P7 ethanol. This is supported by previous studies that showed apoptic markers in transgenically labeled GABA cells immediately after P7 ethanol, in cortex and hippocampus (Bird et al. 2018; Saito et al. 2018). Nevertheless, there is evidence that cell death may only partly explain the loss of GABA cells. A study of

neonatal hypoxia (at P3–P10 in mice) also found about 30% reduction of immunolabeled GABA cells, but did not find a corresponding reduction of GABA cells that were transgenically labeled for GAD67-EGFP. Furthermore, environmental enrichment at juvenile ages reversed the loss of immunolabeled GABA cells (Komitova et al. 2013). Similarly, we previously found that neonatal ethanol caused reduction of PV-immunolabeled cells in P90 barrel cortex, but not of the perineuronal nets that normally colocalized with PV neurons (Saito et al. 2018). These findings suggest that some GABA cells may be present but have suppressed phenotypes following neonatal lesions. While our previous study in barrel cortex showed the reduction of PV cells was delayed until after P14, we did not replicate this delay in the present study, suggesing that PV development in barrel cortex may differ from that of other cortical areas. We also found that reduction of PV cells in dentate gyrus (Saito et al. 2018) and entorhinal cortex (unpublished results) after P7 ethanol occured earlier than in barrel cortex. Our present results in whole neocortex showed that 3 major subtypes of GABA cells are reduced as early as P14. Only CR cells showed trend-level evidence for ethanol-induced reductions that increased at later ages.

Our counts of total neuron number showed that P7 ethanol caused a highly significant 18% reduction at P14, but a similar reduction was not present at P20–30. A transient reduction of cortical neuron number was previously described after neonatal ethanol in rats (Mooney and Napper 2005) and after neonatal hypoxia in mice (Fagel et al. 2006). In the latter study, there was a 30% decrease of neuron number at P11, one day after P3–P10 hypoxia treatment, but at P18 neuron number was not decreased. The authors hypothesized that neonatal neuron loss is compensated by neurogenesis, and in fact they subsequently demonstrated that neonatal hypoxia causes an increase of postnatal neurogenesis, demostrated by BRDU uptake into cortical precursor cells at P15 (Bi et al. 2011). However, they suggested that the modest number of newborn neurons may be insufficent to compensate for the 30% loss of cortical neurons (Salmaso et al. 2014).

An additional mechanism to overcome early neuron loss is suggested by the presence of ongoing programmed cell death. It is plausible that P7 ethanol causes a premature acceleration of programmed cell death, that in control animals continues at a more gradual pace until similar numbers are acheived by about P20. This explanation was previously proposed to explain transient neuron loss in rat visual cortex after neonatal ethanol (Mooney and Napper 2005). It is consistent with the idea that the ethanol and other stimuli easily induce apoptosis at P7 because this is a time when neurons are highly predisposed to undergo programmed cell death (Nikolic et al. 2013). An early stereological study in mouse neocortex estimated that as many as 30% of neurons are lost during normal programmed cell death, with the steepest decline at P5–P10, followed a more gradual decline and stable neuron numbers by P30 (Heumann et al. 1978). Subsequent authors using alternative methods estimated the neuron loss to be 10–20%, in mice (Verney et al. 2000) or greater than 30%, in rats (Bandeira et al. 2009). Studies that mapped the distribution of pyknotic/apoptotic cells in rat or mouse cortex have consistently shown that cell death peaks about P5–7, gradually decreases until about P15, and then continues at low levels as late as P30 (Ferrer et al. 1990; Spreafico et al. 1995; Verney et al. 2000; Nunez et al. 2001; Mosley et al. 2017). These studies indicate that our estimate of 14% decline in neuron number after P8 includes only the latter portion of programmed cell death.

Our different anatomical measurements indicate that neonatal ethanol has multiple effects on cerebral cortex that emerge at different times in posnatal development. An immediate effect within hours of treatment is widespread apoptosis across cortex of many pyramidal and non-pyramidal cells. As early as P14 there is reduction of most types of GABA cells either due to cell death or supressed GABAergic phenotype, that subsequently persists into adulthood. Also by P14 there is a striking reduction of total neuron number, but unlike the deficit of GABA cells this reduction is transient. Cortical volume is also transiently reduced near P14, but unlike neuron number is also robustly reduced in post-adolescent animals. The cellular mechanisms that give rise to this sequence of events remain to be established. Like previous authors, we suggest that transient reduction of total neuron number could be due to an acute acceleration of normally occurring programmed cell death, in addition to increased neurogenesis. At present, the mechanisms that regulate programmed cell death in cortex are incompletely understood. Its disruption could interfere with the normal selection for survival of neurons and cortical connections, leading to subsequent behavioral and developmental deficits. It is notable that although programmed cell death occurs at the same time in GABA cells and pyramidal cells, the mechanisms that regulate their elimination appear to be distinct and independent (Southwell et al. 2012). The differential cell death mechanisms might be associated with the selective reduction of GABA cells by neonatal ethanol.

Acknowledgements This work was supported by a grant from National Institute on Alcohol Abuse and Alcoholism (R01- AA023181) to M.S. and D.A.W.

Compliance with ethical standards

Conflict of interest The authors declare that they do not have financial conflicts of interest that would influence this research.

Ethical standards All procedures were approved by the Nathan Kline Institute IACUC and were in accordance with NIH guidelines for the proper treatment of animals.

References

Archibald SL, Fennema-Notestine C, Gamst A, Riley EP, Mattson SN, Jernigan TL (2001) Brain dysmorphology in individuals with severe prenatal alcohol exposure. Dev Med Child Neurol 43:148–154

Bandeira F, Lent R, Herculano-Houzel S (2009) Changing numbers of neuronal and non-neuronal cells underlie postnatal brain growth in the rat. Proc Natl Acad Sci USA 106:14108–14113

Barger N, Sheley MF, Schumann CM (2015) Stereological study of pyramidal neurons in the human superior temporal gyrus from childhood to adulthood. J Comp Neurol 523:1054–1072

Baribeau DA, Anagnostou E (2013) A comparison of neuroimaging findings in childhood onset schizophrenia and autism spectrum disorder: a review of the literature. Front Psychiatry 4:175

Benros ME, Waltoft BL, Nordentoft M, Ostergaard SD, Eaton WW, Krogh J, Mortensen PB (2013) Autoimmune diseases and severe infections as risk factors for mood disorders: a nationwide study. JAMA Psychiatry 70:812–820

Bi B, Salmaso N, Komitova M, Simonini MV, Silbereis J, Cheng E, Kim J, Luft S, Ment LR, Horvath TL, Schwartz ML, Vaccarino FM (2011) Cortical glial fibrillary acidic protein-positive cells generate neurons after perinatal hypoxic injury. J Neurosci 31:9205–9221

Bird CW, Taylor DH, Pinkowski NJ, Chavez GJ, Valenzuela CF (2018) Long-term Reductions in the Population of GABAergic Interneurons in the Mouse Hippocampus following Developmental Ethanol Exposure. Neuroscience 383:60–73

Brown AS (2011) The environment and susceptibility to schizophrenia. Prog Neurobiol 93:23–58

Cannon JR, Greenamyre JT (2009) NeuN is not a reliable marker of dopamine neurons in rat substantia nigra. Neurosci Lett 464:14–17

Catts VS, Fung SJ, Long LE, Joshi D, Vercammen A, Allen KM, Fillman SG, Rothmond DA, Sinclair D, Tiwari Y, Tsai SY, Weickert TW, Shannon Weickert C (2013) Rethinking schizophrenia in the context of normal neurodevelopment. Front Cell Neurosci 7:60

Coleman LG Jr, Jarskog LF, Moy SS, Crews FT (2009) Deficits in adult prefrontal cortex neurons and behavior following early post-natal NMDA antagonist treatment. Pharmacol Biochem Behav 93:322–330

Coleman LG Jr, Oguz I, Lee J, Styner M, Crews FT (2012) Postnatal day 7 ethanol treatment causes persistent reductions in adult mouse brain volume and cortical neurons with sex specific effects on neurogenesis. Alcohol 46:603–612

Dobbing J, Sands J (1979) Comparative aspects of the brain growth spurt. Early Hum Dev 3:79–83

Dorph-Petersen KA, Nyengaard JR, Gundersen HJ (2001) Tissue shrinkage and unbiased stereological estimation of particle number and size. J Microsc 204:232–246

Dorph-Petersen KA, Pierri JN, Perel JM, Sun Z, Sampson AR, Lewis DA (2005) The influence of chronic exposure to antipsychotic medications on brain size before and after tissue fixation: a comparison of haloperidol and olanzapine in macaque monkeys. Neuropsychopharmacol 30:1649–1661

Dorph-Petersen KA, Delevich KM, Marcsisin MJ, Zhang W, Sampson AR, Gundersen HJ, Lewis DA, Sweet RA (2009) Pyramidal neuron number in layer 3 of primary auditory cortex of subjects with schizophrenia. Brain Res 1285:42–57

Dribben WH, Creeley CE, Farber N (2011) Low-level lead exposure triggers neuronal apoptosis in the developing mouse brain. Neurotoxicol Teratol 33:473–480

Duan W, Zhang YP, Hou Z, Huang C, Zhu H, Zhang CQ, Yin Q (2016) Novel Insights into NeuN: from Neuronal Marker to Splicing Regulator. Mol Neurobiol 53:1637–1647

Duman CH, Duman RS (2015) Spine synapse remodeling in the pathophysiology and treatment of depression. Neurosci Lett 601:20–29

Fagel DM, Ganat Y, Silbereis J, Ebbitt T, Stewart W, Zhang H, Ment LR, Vaccarino FM (2006) Cortical neurogenesis enhanced by chronic perinatal hypoxia. Exp Neurol 199:77–91

Ferrer I, Bernet E, Soriano E, del Rio T, Fonseca M (1990) Naturally occurring cell death in the cerebral cortex of the rat and removal of dead cells by transitory phagocytes. Neuroscience 39:451–458

Ghosal S, Hare B, Duman RS (2017) Prefrontal Cortex GABAergic Deficits and Circuit Dysfunction in the Pathophysiology and Treatment of Chronic Stress and Depression. Curr Opin Behav Sci 14:1–8

Giedd JN, Rapoport JL (2010) Structural MRI of pediatric brain development: what have we learned and where are we going? Neuron 67:728–734

Gogtay N (2008) Cortical brain development in schizophrenia: insights from neuroimaging studies in childhood-onset schizophrenia. Schizophr Bull 34:30–36

Granato A (2006) Altered organization of cortical interneurons in rats exposed to ethanol during neonatal life. Brain Res 1069:23–30

Granato A, Di Rocco F, Zumbo A, Toesca A, Giannetti S (2003) Organization of cortico-cortical associative projections in rats exposed to ethanol during early postnatal life. Brain Res Bull 60:339–344

Gundersen HJG, Bagger P, Bendtsen TF, Evans SM, Korbo L, Marcussen N, Moller A, Nielesen K, Nyengaard JR, Pakkenberg B, Sorensen FB, Vesterby A, West MJ (1988) The new stereological tools: dissector, fractionator, nucleator and point sampled intercepts and their use in pathological research and diagnosis. Acta Pathol Microbiol Immunol Scan 96:857–881

Gundersen HJ, Jensen EB, Kieu K, Nielsen J (1999) The efficiency of systematic sampling in stereology–reconsidered. J Microsc 193:199–211

Hahn ME, Walters JK, Lavooy J, DeLuca J (1983) Brain growth in young mice: evidence on the theory of phrenoblysis. Dev Psychobiol 16:377–383

Hamilton GF, Criss KJ, Klintsova AY (2015) Voluntary exercise partially reverses neonatal alcohol-induced deficits in mPFC layer II/III dendritic morphology of male adolescent rats. Synapse 69:405–415

Hamilton GF, Bucko PJ, Miller DS, DeAngelis RS, Krebs CP, Rhodes JS (2016) Behavioral deficits induced by third-trimester equivalent alcohol exposure in male C57BL/6 J mice are not associated with reduced adult hippocampal neurogenesis but are still rescued with voluntary exercise. Behav Brain Res 314:96–105

Hell S, Reiner C, Cremer C, Stelzer EHK (1993) Aberrations in confocal fluorescence microscopy induced by mismatches in refractive index. J Microsc 169:391–405

Heumann D, Leuba G, Rabinowicz T (1978) Postnatal development of the mouse cerebral neocortex. IV. Evolution of the total cortical volume, of the population of neurons and glial cells. J Hirnforsch 19:385–393

Huttenlocher PR (1990) Morphometric study of human cerebral cortex development. Neuropsychologia 28:517–527

Huttenlocher PR, Dabholkar AS (1997) Regional differences in synaptogenesis in human cerebral cortex. J Comp Neurol 387:167–178

Ieraci A, Herrera DG (2007) Single alcohol exposure in early life damages hippocampal stem/progenitor cells and reduces adult neurogenesis. Neurobiol Dis 26:597–605

Ikonomidou C, Bittigau P, Ishimaru MJ, Wozniak DF, Koch C, Genz K, Price MT, Stefovska V, Horster F, Tenkova T, Dikranian K, Olney JW (2000) Ethanol-induced apoptotic neurodegeneration and fetal alcohol syndrome. Science 287:1056–1060

Inta D, Alfonso J, von Engelhardt J, Kreuzberg MM, Meyer AH, van Hooft JA, Monyer H (2008) Neurogenesis and widespread

forebrain migration of distinct GABAergic neurons from the postnatal subventricular zone. Proc Natl Acad Sci USA 105:20994–20999

Juraska JM, Willing J (2016) Pubertal onset as a critical transition for neural development and cognition. Brain Res 25:45. https://doi.org/10.1016/j.brainres.2016.04.012

Kim JH, Juraska JM (1997) Sex differences in the development of axon number in the splenium of the rat corpus callosum from postnatal day 15 through 60. Brain Res Dev Brain Res 102:77–85

Komitova M, Xenos D, Salmaso N, Tran KM, Brand T, Schwartz ML, Ment L, Vaccarino FM (2013) Hypoxia-induced developmental delays of inhibitory interneurons are reversed by environmental enrichment in the postnatal mouse forebrain. J Neurosci 33:13375–13387

Kumral A, Tugyan K, Gonenc S, Genc K, Genc S, Sonmez U, Yilmaz O, Duman N, Uysal N, Ozkan H (2005) Protective effects of erythropoietin against ethanol-induced apoptotic neurodegenaration and oxidative stress in the developing C57BL/6 mouse brain. Brain Res Dev Brain Res 160:146–156

Lawrence RC, Otero NK, Kelly SJ (2012) Selective effects of perinatal ethanol exposure in medial prefrontal cortex and nucleus accumbens. Neurotoxicol Teratol 34:128–135

Le Magueresse C, Monyer H (2013) GABAergic interneurons shape the functional maturation of the cortex. Neuron 77:388–405

Lebel C, Mattson SN, Riley EP, Jones KL, Adnams CM, May PA, Bookheimer SY, O'Connor MJ, Narr KL, Kan E, Abaryan Z, Sowell ER (2012) A longitudinal study of the long-term consequences of drinking during pregnancy: heavy in utero alcohol exposure disrupts the normal processes of brain development. J Neurosci 32:15243–15251

Lewin M, Ilina M, Betz J, Masiello K, Hui M, Wilson DA, Saito M (2018) Developmental ethanol-induced sleep fragmentation, behavioral hyperactivity, cognitive impairment and parvalbumin cell loss are prevented by lithium co-treatment. Neuroscience 369:269–277

Lyck L, Kroigard T, Finsen B (2007) Unbiased cell quantification reveals a continued increase in the number of neocortical neurones during early post-natal development in mice. Eur J Neurosci 26:1749–1764

Markham JA, Mullins SE, Koenig JI (2013) Periadolescent maturation of the prefrontal cortex is sex-specific and is disrupted by prenatal stress. J Comp Neurol 521:1828–1843

Melvin NR, Dyck RH (2003) Developmental distribution of calretinin in mouse barrel cortex. Brain Res Dev Brain Res 143:111–114

Miller MW (1988) Maturation of rat visual cortex: iV. The generation, migration, morphogenesis, and connectivity of atypically oriented pyramidal neurons. J Comp Neurol 274:387–405

Miyoshi G, Fishell G (2011) GABAergic interneuron lineages selectively sort into specific cortical layers during early postnatal development. Cereb Cortex 21:845–852

Mooney SM, Napper RM (2005) Early postnatal exposure to alcohol reduces the number of neurons in the occipital but not the parietal cortex of the rat. Alcohol Clin Exp Res 29:683–691

Mosley M, Shah C, Morse KA, Miloro SA, Holmes MM, Ahern TH, Forger NG (2017) Patterns of cell death in the perinatal mouse forebrain. J Comp Neurol 525:47–64

Nagamoto-Combs K, Manocha GD, Puig K, Combs CK (2016) An improved approach to align and embed multiple brain samples in a gelatin-based matrix for simultaneous histological processing. J Neurosci Methods 261:155–160

Nikolic M, Gardner HA, Tucker KL (2013) Postnatal neuronal apoptosis in the cerebral cortex: physiological and pathophysiological mechanisms. Neuroscience 254:369–378

Noel M, Norris EH, Strickland S (2011) Tissue plasminogen activator is required for the development of fetal alcohol syndrome in mice. Proc Natl Acad Sci USA 108:5069–5074

Nunez JL, Lauschke DM, Juraska JM (2001) Cell death in the development of the posterior cortex in male and female rats. J Comp Neurol 436:32–41

O'Donnell P (2011) Adolescent onset of cortical disinhibition in schizophrenia: insights from animal models. Schizophr Bull 37:484–492

Olney JW, Tenkova T, Dikranian K, Qin YQ, Labruyere J, Ikonomidou C (2002a) Ethanol-induced apoptotic neurodegeneration in the developing C57BL/6 mouse brain. Brain Res Dev Brain Res 133:115–126

Olney JW, Tenkova T, Dikranian K, Muglia LJ, Jermakowicz WJ, D'Sa C, Roth KA (2002b) Ethanol-induced caspase-3 activation in the in vivo developing mouse brain. Neurobiol Dis 9:205–219

Petanjek Z, Judas M, Simic G, Rasin MR, Uylings HB, Rakic P, Kostovic I (2011) Extraordinary neoteny of synaptic spines in the human prefrontal cortex. Proc Natl Acad Sci USA 108:13281–13286

Rabinowicz T, de Courten-Myers GM, Petetot JM, Xi G, de los Reyes E (1996) Human cortex development: estimates of neuronal numbers indicate major loss late during gestation. J Neuropathol Exp Neurol 55:320–328

Reich B, Hoeber D, Bendix I, Felderhoff-Mueser U (2016) Hyperoxia and the immature brain. Dev Neurosci 38:311–330

Revishchin AV, Okhotin VE, Pavlova GV (2010) New calretinin-positive cells with polymorphous spines in the mouse forebrain during early postnatal ontogeny. Neurosci Behav Physiol 40:833–840

Sadrian B, Lopez-Guzman M, Wilson DA, Saito M (2014) Distinct neurobehavioral dysfunction based on the timing of developmental binge-like alcohol exposure. Neuroscience 280:204–219

Saito M, Mao RF, Wang R, Vadasz C, Saito M (2007) Effects of gangliosides on ethanol-induced neurodegeneration in the developing mouse brain. Alcohol Clin Exp Res 31:665–674

Saito M, Smiley JF, Hui M, Masiello K, Betz J, Ilina M, Saito M, Wilson DA (2018) Neonatal ethanol disturbs the normal maturation of parvalbumin interneurons surrounded by subsets of perineuronal Nets in the Cerebral Cortex: Partial Reversal by Lithium. Cereb Cortex 29:1383–1397

Salmaso N, Jablonska B, Scafidi J, Vaccarino FM, Gallo V (2014) Neurobiology of premature brain injury. Nat Neurosci 17:341–346

Schneider M (2013) Adolescence as a vulnerable period to alter rodent behavior. Cell Tissue Res 354:99–106

Semple BD, Blomgren K, Gimlin K, Ferriero DM, Noble-Haeusslein LJ (2013) Brain development in rodents and humans: identifying benchmarks of maturation and vulnerability to injury across species. Prog Neurobiol 106–107:1–16

Shaw P, Greenstein D, Lerch J, Clasen L, Lenroot R, Gogtay N, Evans A, Rapoport J, Giedd J (2006) Intellectual ability and cortical development in children and adolescents. Nature 440:676–679

Smiley JF, Bleiwas C (2012) Embedding matrix for simultaneous processing of multiple histological samples. J Neurosci Methods 209:195–198

Smiley JF, Rosoklija G, Mancevski B, Mann JJ, Dwork AJ, Javitt DC (2009) Altered volume and hemispheric asymmetry of the superficial cortical layers in the schizophrenia planum temporale. Eur J Neurosci 30:449–463

Smiley JF, Saito M, Bleiwas C, Masiello K, Ardekani B, Guilfoyle DN, Gerum S, Wilson DA, Vadasz C (2015) Selective reduction of cerebral cortex GABA neurons in a late gestation model of fetal alcohol spectrum disorder. Alcohol 49:571–580

Southwell DG, Froemke RC, Alvarez-Buylla A, Stryker MP, Gandhi SP (2010) Cortical plasticity induced by inhibitory neuron transplantation. Science 327:1145–1148

Southwell DG, Paredes MF, Galvao RP, Jones DL, Froemke RC, Sebe JY, Alfaro-Cervello C, Tang Y, Garcia-Verdugo JM, Rubenstein JL, Baraban SC, Alvarez-Buylla A (2012) Intrinsically

determined cell death of developing cortical interneurons. Nature 491:109–113
Spear LP (2000) The adolescent brain and age-related behavioral manifestations. Neurosci Biobehav Rev 24:417–463
Spreafico R, Frassoni C, Arcelli P, Selvaggio M, De Biasi S (1995) In situ labeling of apoptotic cell death in the cerebral cortex and thalamus of rats during development. J Comp Neurol 363:281–295
Subbanna S, Shivakumar M, Psychoyos D, Xie S, Basavarajappa BS (2013) Anandamide-CB1 receptor signaling contributes to postnatal ethanol-induced neonatal neurodegeneration, adult synaptic, and memory deficits. J Neurosci 33:6350–6366
Suri D, Teixeira CM, Cagliostro MK, Mahadevia D, Ansorge MS (2015) Monoamine-sensitive developmental periods impacting adult emotional and cognitive behaviors. Neuropsychopharmacology 40:88–112
Susick LL, Lowing JL, Bosse KE, Hildebrandt CC, Chrumka AC, Conti AC (2014) Adenylyl cylases 1 and 8 mediate select striatal-dependent behaviors and sensitivity to ethanol stimulation in the adolescent period following acute neonatal ethanol exposure. Behav Brain Res 269:66–74
Uylings HB (2000) Development of the cerebral cortex in rodents and man. Eur J Morphol 38:309–312
Verney C, Takahashi T, Bhide PG, Nowakowski RS, Caviness VS Jr (2000) Independent controls for neocortical neuron production and histogenetic cell death. Dev Neurosci 22:125–138
Wagner JL, Zhou FC, Goodlett CR (2014) Effects of one- and three-day binge alcohol exposure in neonatal C57BL/6 mice on spatial learning and memory in adolescence and adulthood. Alcohol 48:99–111
Willing J, Juraska JM (2015) The timing of neuronal loss across adolescence in the medial prefrontal cortex of male and female rats. Neuroscience 301:268–275
Wilson DA, Peterson J, Basavaraj BS, Saito M (2011) Local and regional network function in behaviorally relevant cortical circuits of adult mice following postnatal alcohol exposure. Alcohol Clin Exp Res 35:1974–1984
Wilson DA, Masiello K, Lewin MP, Hui M, Smiley JF, Saito M (2016) Developmental ethanol exposure-induced sleep fragmentation predicts adult cognitive impairment. Neuroscience 322:18–27
Wozniak DF, Hartman RE, Boyle MP, Vogt SK, Brooks AR, Tenkova T, Young C, Olney JW, Muglia LJ (2004) Apoptotic neurodegeneration induced by ethanol in neonatal mice is associated with profound learning/memory deficits in juveniles followed by progressive functional recovery in adults. Neurobiol Dis 17:403–414
Zuo Y, Lin A, Chang P, Gan WB (2005) Development of long-term dendritic spine stability in diverse regions of cerebral cortex. Neuron 46:181–189